INTERNAL STRAIN SENSING IN CARBON FIBRE COMPOSITES VIA DIGITAL VOLUME CORRELATION AND *IN SITU* SYNCHROTRON COMPUTED TOMOGRAPHY

Y. Lee[1*], K. Rankin[1], P. Patel[2], P. Basford[1], C. Furtado[3], P. Campos[3], A. Takeuchi[4], M. Uesugi[4], B. Wardle[2], M. Jalalvand[1], M.N. Mavrogordato[1], S.M. Spearing[1], I. Sinclair[1]
[1] Engineering Materials, Faculty of Engineering and Physical Sciences, University of Southampton, Southampton, UK, yeajin.lee@soton.ac.uk and www.southampton.ac.uk
[2] Department of Mechanical Engineering, Massachusetts Institute of Technology, Cambridge, Massachusetts, USA, palak@mit.edu and www.mit.edu
[3] Department of Mechanical Engineering, University of Porto, Porto, Portugal, cfurtado@fe.up.pt and www.up.pt
[4] Japan Synchrotron Radiation Research Institute (JASRI/Spring-8), Sayo, Japan, uesugi@spring8.or.jp and www.spring8.or.jp

Keywords: DVC, *In situ* SRCT, Strain redistribution, Ineffective length

ABSTRACT

Digital Volume Correlation (DVC) is a powerful non-intrusive technique capable of volumetric full-field strain mapping of internal structures via displacement tracking. This study, a combination of DVC and *in situ* Synchrotron Radiation Computed Tomography (SRCT), introduces Silicon Dioxide (SiO_2) particles into carbon fibre-reinforced polymers to extend the utilisation of DVC technique to more industrially relevant materials, where detailed sequences of fibre breaks and their accumulation can be identified down to the individual fibre level. The DVC analysis with strain mapping explores the process of strain redistribution longitudinally from fibre breaks that occur under quasi-static tensile loading for various load levels. It is shown that the newly developed material not only exhibits a comparable level of DVC performance to the previous study using $BaTiO_3$ particles, but also attains improved particle distribution with reduced agglomeration. The scale/extent of strain disturbances around individual fibre breaks is compared for multiple sites, suggesting reasonable consistency and confidence in mapping ineffective lengths.

1 INTRODUCTION

A fundamental understanding of the fibre break process is essential for a complete interpretation of composite tensile failure, alongside the various other composite damage mechanisms (*e.g.*, fibre-matrix interfacial de-bonding, fibre pull-out, matrix micro-cracking, delamination, sub-laminate, etc.). Under tension, local load transfer around individual fibre break plays an important role in determining the ultimate tensile failure of composite materials. This principally occurs by inducing shear stress and strain in the matrix around individual fibre breaks, followed by load transfer into adjacent fibres, bypassing the broken fibres [1]. With ongoing loading, a critical cluster of fibre breaks is thought to form in an unstable, self-sustained manner when sufficient breaks are accumulated, leading to catastrophic failure [2]. Consequently, understanding the stress redistribution around fibre breaks and the length over which load transfer occurs (*i.e.*, ineffective length) is critical when predicting tensile failure of unidirectional (UD) composites.

Advances in X-ray Computed Tomography combined with *in situ* mechanical testing has allowed the identification of detailed sequences of damage accumulation down to the fibre level, in 3D, within the bulk of real engineering materials under load. DVC combined with *in situ* Synchrotron Radiation Computed Tomography has become a powerful non-intrusive technique capable of quantifying full-field behaviour of internal structures between different load states by extracting local displacements, and hence internal strains. However, the main intrinsic DVC challenges associated with conventional UD CFRPs are attributed to their somewhat self-similar/regular microstructures and featureless fibre surfaces, particularly along the fibre direction, resulting in potentially false correlation peaks and displacement inaccuracies, particularly in the fibre direction.

Recent work by Schöberl *et al.* [1, 2] demonstrated the principle of high-resolution DVC combined with *in situ* SRCT tensile testing, capable of fibre-level strain mapping, by embedding a sparse population of 400 nm $BaTiO_3$ particles within the matrix of carbon fibre-epoxy composites. This DVC approach enabled 3D volumetric strain field assessment at fibre breaks in UD CFRPs. The use of such a high atomic number material, imaged at high resolution of 0.65 μm, proved the feasibility of DVC for fibre break strain mapping. However, a degree of particle inhomogeneity remained after manufacturing (particle clusters/clumps), along with contrast artefacts in places (streaks).

Accordingly, it is desirable to identify alternative particle materials that can offer a comparable or higher level of DVC performance to $BaTiO_3$ particles, whilst minimising potentially detrimental effects of particle inhomogeneity on: (a) DVC performance, and (b) disturbance of fibre position/alignment. This work will present the introduction of industrial-grade SiO_2 particles with a nominal diameter of 500 nm for the purpose of extending the utilisation of DVC technique to industrially relevant materials while exploiting four attributes: (1) SiO_2 particles are closer to the type of particles that might be used at ply interfaces, (2) they are routinely utilised in practice as a filler in polymer materials to increase the effective modulus and strength, (3) reasonably uniform particle distributions are expected to be achievable, (4) the lower atomic number constituents should reduce the presence of certain imaging artefacts. Understanding of the strain redistribution process surrounding fibre breaks will be discussed, along with the evaluation of the DVC applicability to the presented material.

2 MATERIALS AND METHODOLOGY

2.1 MATERIALS

Cross-ply laminates of carbon fibre pre-preg were prepared by Mitsubishi Chemical Corporation with a $[90_2/0_2]_s$ configuration, total thickness of ~1mm, and nominal fibre volume fraction of ~0.55. Curing was carried out via a standard aerospace autoclave cycle to the manufacturer's specifications. Nominal fibre diameter was 5.4 μm, with a tensile modulus 286 GPa. The surface of the carbon fibres was treated to control the adhesion between the matrix/fibre interfaces. As shown in **Table. 1**, two different configurations of surface treatments were tested, with type *I* providing stronger adhesion than *II*, while other material specifications (*e.g.*, sizing agent) remained the same.

Material Configuration	**Fibre diameter** [μm]	**Sizing agent type**	**Surface treatment type**	**Concentration of SiO_2 particles** [wt %]	**Resin**	**Nominal average UTS** [MPa]	
						Ex situ	*In situ*
A	5.4	Same	II	10	Epoxy	2993	2963
B			I			3060	2846
A'			II	N/A		3162	2958
B'			I			3292	2966

Table. 1. Summary of the material configurations assessed in this work

To enable local DVC analysis on the self-similar CFRP microstructure, it is essential to produce a distinct grey-level distribution within the relevant images. Consequently, the epoxy-resin was filled with surface-treated SiO_2 particles of spherical geometry with a stated mean diameter of 500 nm. The concentration of particle doping was limited to ~10 wt% of the epoxy-resin to minimise influences on mechanical behaviour, particularly damage mechanisms. For both materials A and B, measurements of ultimate tensile strength (UTS) were initially carried out to evaluate whether the particles affect the macroscopic mechanical behaviour when compared to particle-free (undoped) materials A' and B'. Under a tensile load, the UTS of a $[90_2/0_2]_s$ CFRP laminate is expected to be primarily determined by tensile failure of the 0° plies. Hence, only the cross-sectional area of the 0° plies was considered in calculating the UTS. The UTS measurements from *in situ* double-edge notched tension (DENT) testing, as presented in **Table. 1**, revealed that the nominal average UTS values of both particle-doped and undoped materials were nearly identical, at ~2900 MPa, indicating that the particle inclusion did not have a significant effect on the strength of the materials. In addition, no significant defects (porosity or gross resin-rich regions) were observed in CT images captured using a resolution of 0.5 μm. As can be seen in **Fig. 1**, raw CT slices of SiO_2 particle-doped materials exhibit a finely, well-dispersed particle distribution (*cf.* the $BaTiO_3$ doped material).

DENT specimens were machined via waterjet cutting, as reported by Wright *et al.* [3]. CT images of each specimen prior to experiment revealed negligible damage and defects from the cutting process [3, 4]. The specimen geometry, as illustrated in **Fig. 2**, was selected following the previous works of Schöberl *et al.* and Rosini *et al.* [1, 2, 5-7]. Both ends of the T-shaped sections of the specimen were attached with 1.5 mm thick aluminium T-tabs. Aerospace-grade level of adhesive, Scotch-Weld™ EC-9323 B/A (3M Company, Maplewood, MN, USA), was used to bond T-tabs on the CFRP surface [8].

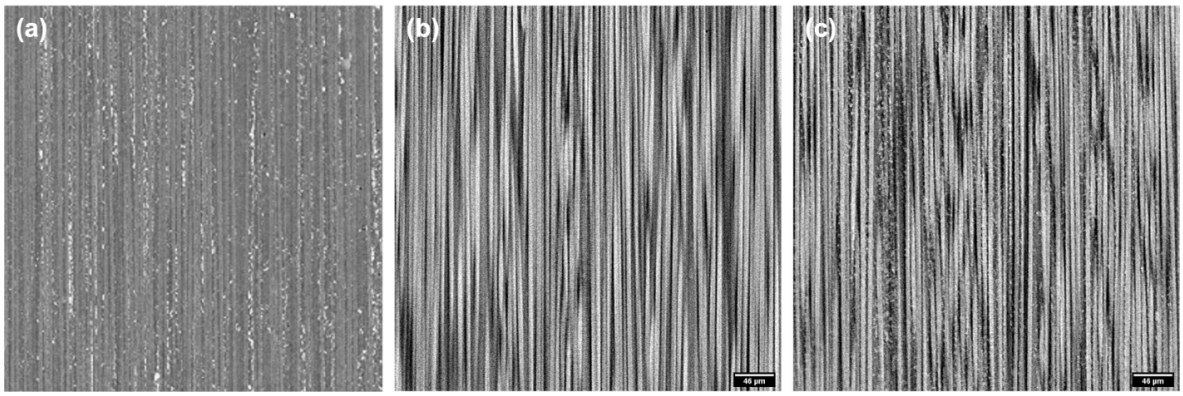

Fig. 1. Example of (a) micro-CT 2D slice showing the distribution of $BaTiO_3$ particles in the CFRPs [5] (b) SRCT 2D slice of SiO_2 particle-free CFRPs (c) SRCT 2D slice showing the distribution of SiO_2 particles in the CFRPs.

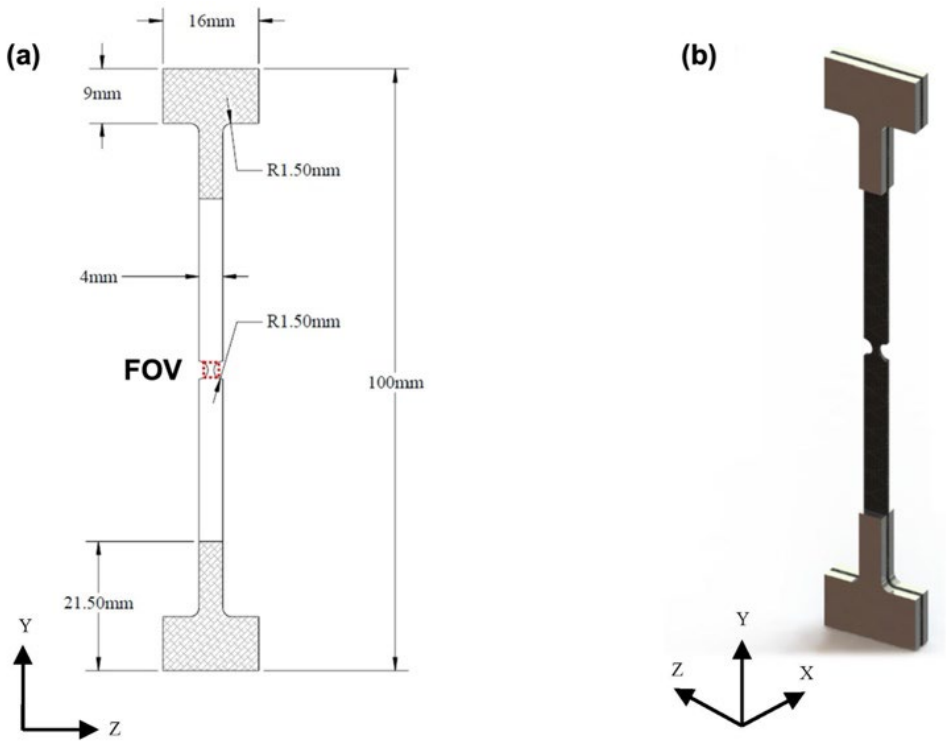

Fig. 2. Double-edge notched tensile specimen: (a) the key specimen dimensions and the field of view at the centre notch area. (b) specimens assembled with aluminium T tabs for *in situ* DENT testing [1].

2.2 SYNCHROTRON RADIATION COMPUTED TOMOGRAPHY (EXPERIMENTAL PROCEDURE)

In situ SRCT tensile tests were performed at the Super Photon ring-8 GeV (Spring-8) BL20XU beamline (Sayo, Japan). As depicted in **Fig. 3**, a modified CT5000 single-actuator electromechanical rig (Deben Ltd., Woolpit, Suffolk, UK) was used to perform the tests. To conduct stepwise *in situ* measurements, loading was carried out at a displacement rate of 0.2 mm/min up to each prescribed load stage, corresponding to ~10%, 80%, 90%, 95%, 98% of the nominal average DENT UTS. Smaller load increments were made at higher loads, as the likelihood of fibre breakage and its accumulation increases exponentially [9]. To ameliorate potential relaxation effects during image acquisition, the applied load was reduced by ~10% from the most recently applied peak level, with the central notched region of the specimen being scanned at this slightly reduced level. As such, the sample would be mechanically stable and any cracks held open to assist in their detection/measurement. Simple repeat scans were carried out under both static (*i.e.*, stationary) and rigid body displacement (RBD) conditions (see §4.1), where load was maintained at the lowest/preload level of 10% of UTS (*i.e.,* the sample being mechanically stable for the scans, but otherwise experiencing no change in stress/strain).

A 2048 × 2048 pixel CCD camera was used with a pixel size of 0.5 μm, resulting in a field of view of ~1.02 mm. A double crystal monochromator (*i.e.,* monochromatic beam) was used with an energy of 28 keV, and each scan acquired 1800 projections at an exposure time of 100 ms. CT image acquisition was performed over a 180° at a sample-to-detector (*i.e.* propagation) distance of ~25 mm.

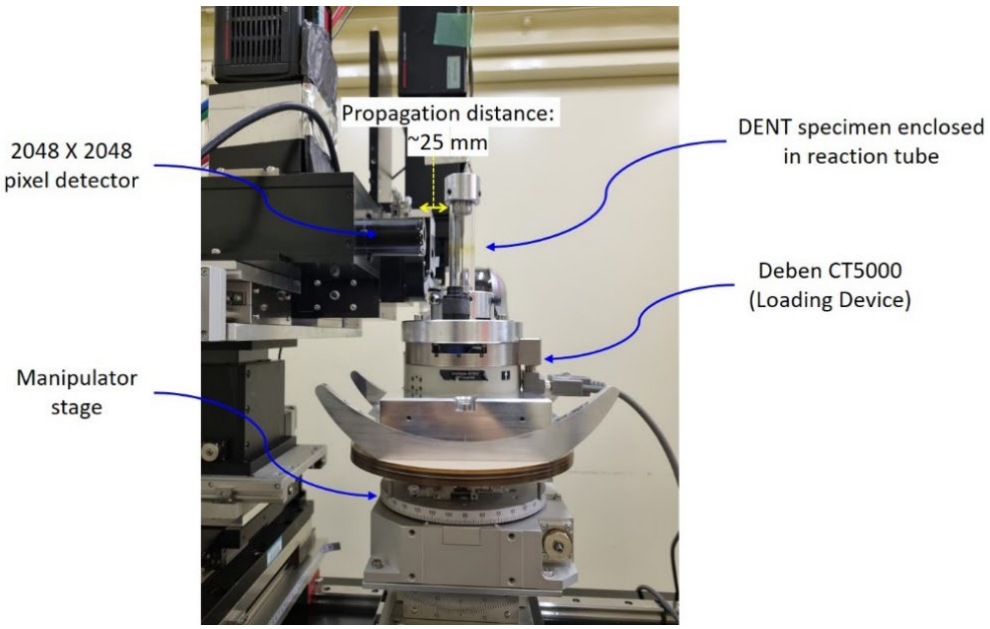

Fig. 3. Experimental configurations of *in situ* DENT testing using the modified DEBEN CT5000 loading rig at Spring-8 BL20XU beamline.

3 DIGITAL VOLUME CORRELATION DESCRIPTION

DVC was performed on the reconstructed volume using the commercial Davis v10.2.0 software (LaVision Ltd., Göttingen, Germany). The overview of the DVC process between two adjacent volumes 'P' and 'Q' is schematically illustrated in **Fig. 4**. The DVC input preparation involves selecting a specific volume of interest (*i.e.,* VOI at which volumetric displacement is calculated) within a set of undeformed and deformed CT volumes to be correlated. The measurement volume is then divided into smaller cubic-shaped sub-volumes based on the desired final sub-set size and an overlap percentage. The contrast pattern of doped particles within each sub-volume, based on variations in their grey-level intensity distributions, is tracked independently from the reference (*i.e.,* undeformed) to the deformed state [10]; for example, a single reference sub-volume with centroid $\boldsymbol{\kappa_0}$ will systematically search the

corresponding sub-volume $\boldsymbol{\kappa}$ in the deformed volume. As a result of the correlation, the local 3D shift (displacement) vector $\boldsymbol{t}$ will be determined from each centroid of both volumes. Finally, 3D full-field strain vector fields can be estimated with numerical derivatives of the vector fields, through a centred finite difference scheme [10-12].

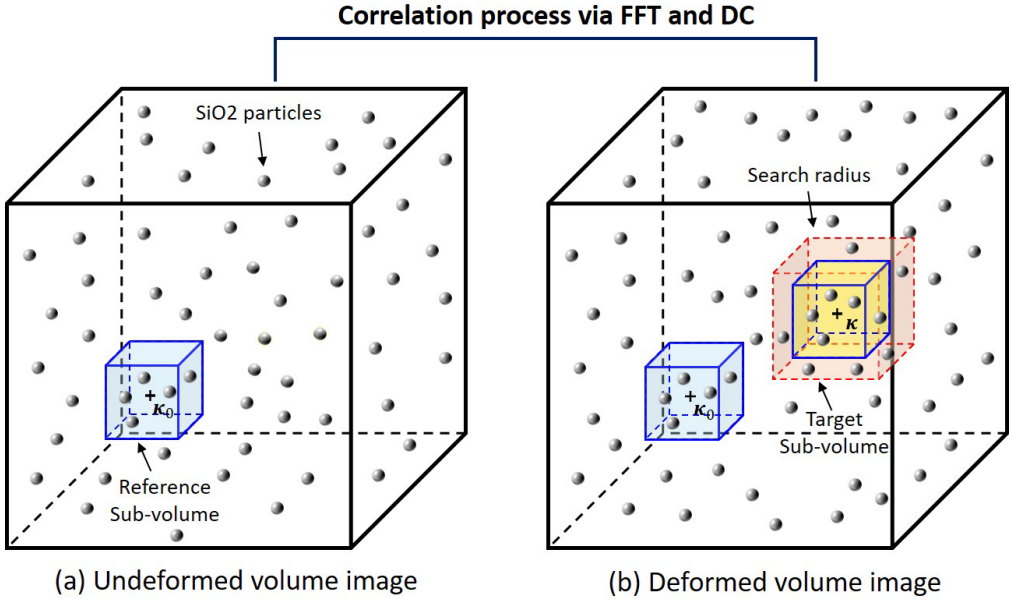

Fig. 4. Schematic diagram of the DVC process implemented by FFT and DC methods between (a) undeformed volume image and (b) deformed volume image. Adapted from Xu *et al*. [12] and Schöberl *et al*. [1].

In this work, the correlation algorithm utilises a multi-step and multi-pass strategy to identify matched sub-volumes; a Fast Fourier Transform (FFT) is first implemented for a global pre-shift, followed by Direct Correlation (DC) for successive refinement. The FFT searches large movements of particles in the deformed state, such as rigid body displacement, by using larger sub-volumes. The range of DC implementation is confined to a specific set of input parameters (*e.g.*, search radius, subset size, number of pass, overlapping value, etc), which allows refinement of sub-volumes to obtain more precise local displacements.

DVC input parameters used for correlation are presented in **Table. 2**. The correlation was processed by one FFT and three DC steps successively. The sub-volume size during the DC steps was incrementally reduced from 64 voxels to 48 voxels, and ultimately determined to be 32 voxels. Concurrently, the search radius was also decreased in every correlation. In finite sub-volume based correlation, spatial sampling issues may affect the accuracy of DVC measurements. As one solution, the overlapping between the adjacent sub-volumes was set to 75% to achieve higher spatial resolution. The 'relative-to-first' correlation mode was chosen, implying that reference recorded at a minimum load was used sequentially for all correlations.

	Final sub-volume size	FFT pre-shift	Step 1 (voxels)	Step 2 (voxels)	Step 3 (voxels)	No.of passes step 1-3	Voxel binning step 1	Voxel binning step 2	Voxel binning step 3
1	32	64	64	40	32	2	4 x 4 x 4	2 x 2 x 2	None
2	40	80	80	48	40				
3	48	80	80	56	48				
4	52	80	80	56	52				
5	64	96	96	80	64				
6	80	128	128	96	80				
7	96	160	160	112	96				
8	104	160	160	112	104				
9	128	176	176	136	128				

Table. 2. Summary of DVC input parameters

A DVC study combined with *in situ* SRCT necessitates quantification of uncertainties (particularly the noise floor), such as intrinsic noise and bias that may arise from the imaging system or surrounding environment, to determine the range of reliability in the DVC strain measurement results associated with fibre breaks. Hence, sets of volumes measuring 600 × 600 × 600 voxels were cropped from the 0° plies in each of the static, RBD, and *in situ* DENT scans. During the volume cropping procedure, attempts were made to avoid the presence of CT artefacts and/or individual grossly misaligned fibres as much as possible. To accelerate correlation time, all DVC volume datasets in 16-bit format were converted to 8-bit format based on previous works [1,13].

4 RESULTS AND DISCUSSIONS

4.1 NOISE AND SENSITIVITY

A DVC study combined with *in situ* SRCT necessitates quantification of uncertainties (*i.e.,* noise floor), such as intrinsic noise and bias that may arise from the imaging system or surrounding environment. Under ideal conditions, the DVC-measured displacement vector fields and computed strains should be zero, with any signal detected, therefore, being artificial. This is also essential to determine the range of reliability in the DVC strain measurement results associated with fibre breaks.

In this study, the noise quantification method is to measure the standard deviation of the DVC-measured strain components within the CT volume. Accordingly, two zero-strain pair analyses were performed in accordance with previous works [1]. The first was a static noise test (SNT), where the same specimen was repeatedly scanned at the same field of view (FOV) position without any alterations in load and CT parameters. The second test was a rigid body displacement in which the specimen was moved parallel to the loading (0°) direction by a pre-defined displacement. A series of scans were performed between each specimen position to evaluate the effect of noise induced during translation on the magnitude of the displacement fields. In the results of DVC-measured strains, any values away from zero are regarded as the noise floor. This method is advantageous for measuring stochastic noise and bias in imaging systems without overestimating errors.

4.1.1 STATIC NOISE TEST

A comparison of the noise floor for materials A and B determined by the static noise tests is presented in **Fig. 5**. The normal strain of 'ε_{yy}', parallel to the fibre load direction, is of particular interest as major fibre breaks occur parallel to the fibre direction. The strains measured by DVC algorithms represent spatially filtered datasets based on the sub-volume size (*i.e.,* spatial resolution), rather than the true strain values. Therefore, the noise floor is also compared for different sub-volume size to observe the compromise between strain and spatial resolution, as reported in the literature [1].

As illustrated in **Fig. 5**, it can be found that the noise floor exhibits a decreasing trend as the sub-volume size increases. This represents a compromise between strain and spatial resolution; the larger the sub-volume size, the lower the spatial resolution in the process of averaging the displacements of all the voxels contained within the sub-volume. In contrast, the use of smaller sub-volumes will compromise strain resolution (*i.e.,* higher errors in displacement measurement) as they may contain fewer particles to be used as displacement trackers [14].

Material configurations 'A' and 'B', differing only in surface treatment type, show the noise floors of ~0.35% and ~0.16%, respectively, when a sub-volume size of 32 voxels is used. The noise floor results from the present study are compared with those of CFRPs doped with 7.5wt% $BaTiO_3$ particles with diameter of 400 nm whose DVC applicability has already been verified by Schöberl *et al*. [1, 2]. As anticipated, the noise floors of SiO_2 doped CFRPs follow the similar decreasing trend for the increase in sub-volume size, as seen in $BaTiO_3$ doped CFRPs. The introduction of SiO_2 particles resulted in a higher noise floor in materials 'A' and 'B', compared to the noise floor of 0.085% in $BaTiO_3$ doped CFRPs when using a sub-volume of 32. Whilst SiO_2 particles are seen to not be as effective as $BaTiO_3$ particles in reducing the noise floor level, all noise floor levels are at least still in the same order of magnitude for both particle types. As such, it can be seen that the use of SiO_2 particles can still provide a technically useful level of DVC performance compared to $BaTiO_3$ doped CFRPs, whilst the SiO_2 demonstrates a more uniform distribution and less disturbance of fibre packing. DVC analysis with SiO_2

particles reveals an effective noise-floor that is significantly lower than the local strains previously measured at fibre breaks [1]. The performance of $BaTiO_3$ doping is in the first instance readily identifiable with the greater X-ray contrast, with reduced contrast of the SiO_2 presenting greater potential for false/erroneous correlations. It is of interest that the two SiO_2 doped CFRPs can be expected to be functionally similar in these tests (*i.e.,* particles being distributed by the same means, in the same matrix, with fibres of equivalent imaging properties). However, the differences observed in Materials A and B in Fig. 5 imply that batch-to-batch process variation in particle distribution may affect DVC performance, hence noise trials for each for each material/batch process combination are recommended.

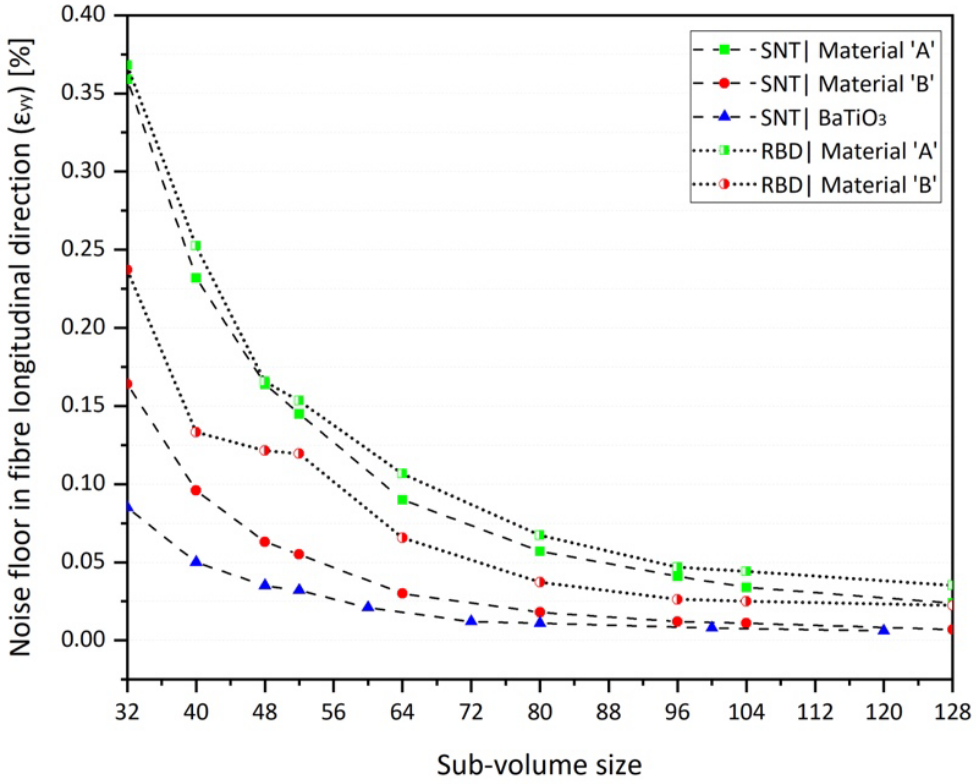

Fig. 5. Noise floor comparison and validation under static noise test and rigid body displacement (zero strain) in three different material systems: SiO_2 doped CFRPs with two different surface treatment types (Material 'A' and Material 'B'), and $BaTiO_3$ doped CFRPs. SNT results of $BaTiO_3$ containing materials are from Schöberl *et al*. [1]

4.1.2 RIGID BODY DISPLACEMENT

The DVC algorithm, using a 32 voxel sub-volume size and 75% overlap, computed the displacement fields and the errors induced while the specimen was rigidly translated parallel to the tensile loading direction (*i.e.,* Y-axis) by a pre-defined displacement of 2.75 µm. The DVC measurement was taken solely in the longitudinal direction, similarly to the SNT. As a result, the average RBD-induced error in Y-displacement was calculated to be 2.515 µm. Following the approach used in Schöberl *et al.*, the induced Y-displacement was manually confirmed by measuring the distance between a unique feature (*e.g.*, a void or SiO_2 particles) and a reference point in Fiji ImageJ™ [15]. The measured Y-displacement falls within the range of 2.75 ± 0.5 µm, with a degree of variation that can be deemed negligible.

A summary of the SNT and RBD corrected errors for different sub-volume sizes is represented in **Fig. 5**. As in the SNT results, the magnitude of the RBD corrected errors in materials 'A' and 'B' were also higher than the value of 0.088% found in $BaTiO_3$ doped CFRPs when using a sub-volume of 32 [1]. The difference in errors are still usefully within the same order of magnitude, as explained in §4.1.1. As may be anticipated the two stationary tests revealed that RBD induces slightly greater error than SNT in SiO_2 doped CFRPs, but is not an overwhelming effect.

4.2 STRAIN FIELD ASSESSMENT AT SINGLE FIBRE BREAKS

As detailed in §4.1.1, the DVC algorithm applies spatial filtering to the real local strains within the material based on the selected sub-volume size and correlation algorithm choices. In other words, the DVC measurement accuracy of local deformation is highly influenced by the volumetric data used for strain calculation at a specific location. Schöberl *et al.* [1] presented a method of using algorithmic masks for fibre breaks to isolate them during the correlation process. The underlying rationale is that no strains can be determined at a break site where there is no material (*e.g.*, fibre break opening, cracks, voids). However, this study opted for correlating volumes without masking the break sites as the effect of masking on the measured longitudinal strains was observed to be insignificant. Furthermore, the primary interest of the work is detecting the distance *away* from a break at which strains return to their background levels, rather than precise mapping of strain field *close in* to a given break.

Fig. 6 presents representative DVC strain maps overlaid with the microstructure for material 'A', which were subjected to *in situ* tensile loading of ~1130 N equivalent to ~90% UTS. The FOV sized ~85 µm × ~85 µm was centred on a singlet (identified by as '#4' in this study), observed as a non-interacting fibre break. To attain the best possible spatial resolution with a comparable level of noise, strain fields were computed using the smallest sub-volume size of 32 voxels (16 µm) and 75% overlap, resulting in a step size of 8 voxels (4 µm). It should be noted that no smoothing via changes in virtual strain gauge size was applied to the measured strains. The far-field strain was computed via DVC at each load step level by taking the average of all the measured strains in the sub-volume.

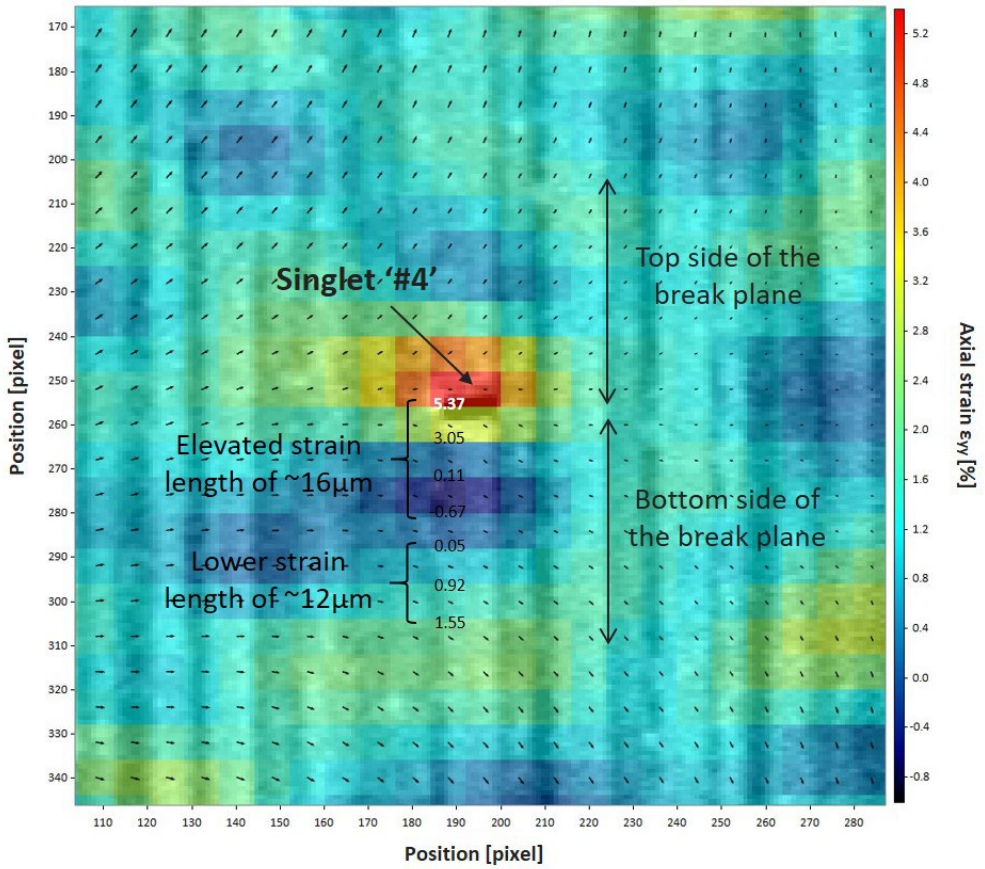

Fig. 6. Example of a DVC strain map illustrating the longitudinal strain fields 'ε_{yy}' surrounding the singlet '#4' in the material 'A', with a far-field strain reaching ~1.16%. FOV is ~85 µm × ~85 µm.

The objective of this study is to understand the strain redistribution process around fibre breaks in the fibre load direction, specifically an analysis of the ineffective length (*i.e*. the length over which 90% of strain recovery occurs). **Fig. 6** illustrates the longitudinal strain gradients exhibiting a nearly symmetrical pattern from the fibre break plane. Numerical data on the longitudinal strains were extracted

longitudinally from the overlapped sub-volumes that were aligned with the centre of the broken fibre. Similar to the results from $BaTiO_3$ doped CFRP [1], each individual line plot shows a consistent trend of increasing or decreasing strain gradients with longitudinal distance changes from break region. However, appreciable variations can be observed in the individual strain distributions, along with a degree of variability in the strain remote from the breaks. Local variations may be attributed to a number of factors, including: low correlation is in sub-volumes containing fibre breaks due to the insufficient amounts of particles, measurement noise, microstructural variations, and different damage mechanisms being involved or superposed on each side of the break plane.

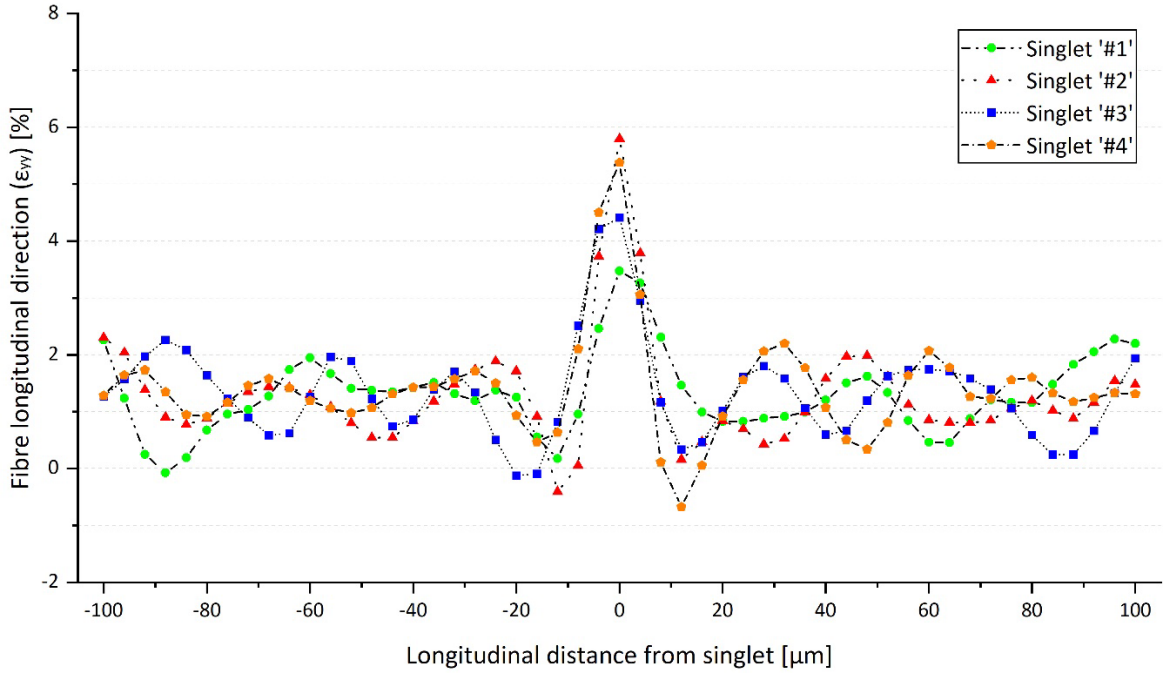

Fig. 7. Collection of the longitudinal strain gradients 'ε_{yy}' of four distinct singlets in the material 'A' at the ~90% UTS level, measured from both sides of the fibre break plane.

To mitigate the effects of local measured variations on the strain distribution measurements, a method of averaging and 'folding' has been applied. To this end, strain distributions are presumed to be symmetrical above and below the break plane, with the top side of the longitudinal strains from eight individual singlets being averaged with equidistant strains measured to the opposite side of the breaks. The corresponding strain data against the distance was collected from 8 individual break sites, all of which were then averaged together. It should be noted that this approach to mitigate variations was carried out while checking the consistency of the ineffective length for the number of fibre breaks being averaged. As **Fig. 8** shows, the resulting line plot 'ε_{yy}' for both material 'A' and 'B' exhibits two distinct strain regions at the 90% UTS level. A tensile peak is identified at the break site, covering a distance of ~16 µm (identified in **Fig. 8** as an 'elevated strain length'), and a 'lower strain length' of ~12 µm, over which strains lower than the far-field value are returned.. The longitudinal distance combining these two strain regions represents a half ineffective length (*i.e.* half-recovery length) on one side of the break. Background/far-field strain variations are seen to be much reduced, as would expected by averaging, with Materials A and B then exhibiting a half ineffective length of 28µm, with similar distances for the elevated and lower strain lengths. The fact that both materials exhibit a very similar full-recovery length suggests that surface treatment differences may not be a critical factor in determining the ineffective length in this system, at least based on this evidence from single fibre breaks at the 90% UTS level. With a comparable level of DVC applicability, industrial-grade SiO_2 containing CFRPs result in a shorter half ineffective length than the previously evaluated in $BaTiO_3$ doped CFRP (reported as ~36 µm): the underlying materials in each case had different carbon fibres, fibre fraction, surface treatments and

manufacturing process, so are not directly comparable, but it is interesting to note that the measured half ineffective lengths are of a similar order (circa 30 µm).

As the load increases, the evolution of eight singlets ('#1-8') in material 'A' and 'B' has been identified, accompanied by an increasing number of adjacent fibre breaks and an increase in the fibre break opening distance (**Fig. 9**). Ongoing comprehensive analysis will take into account any corresponding changes in ineffective length with increasing load, and also evidence of load coupling and shedding around and between multiple-break sites.

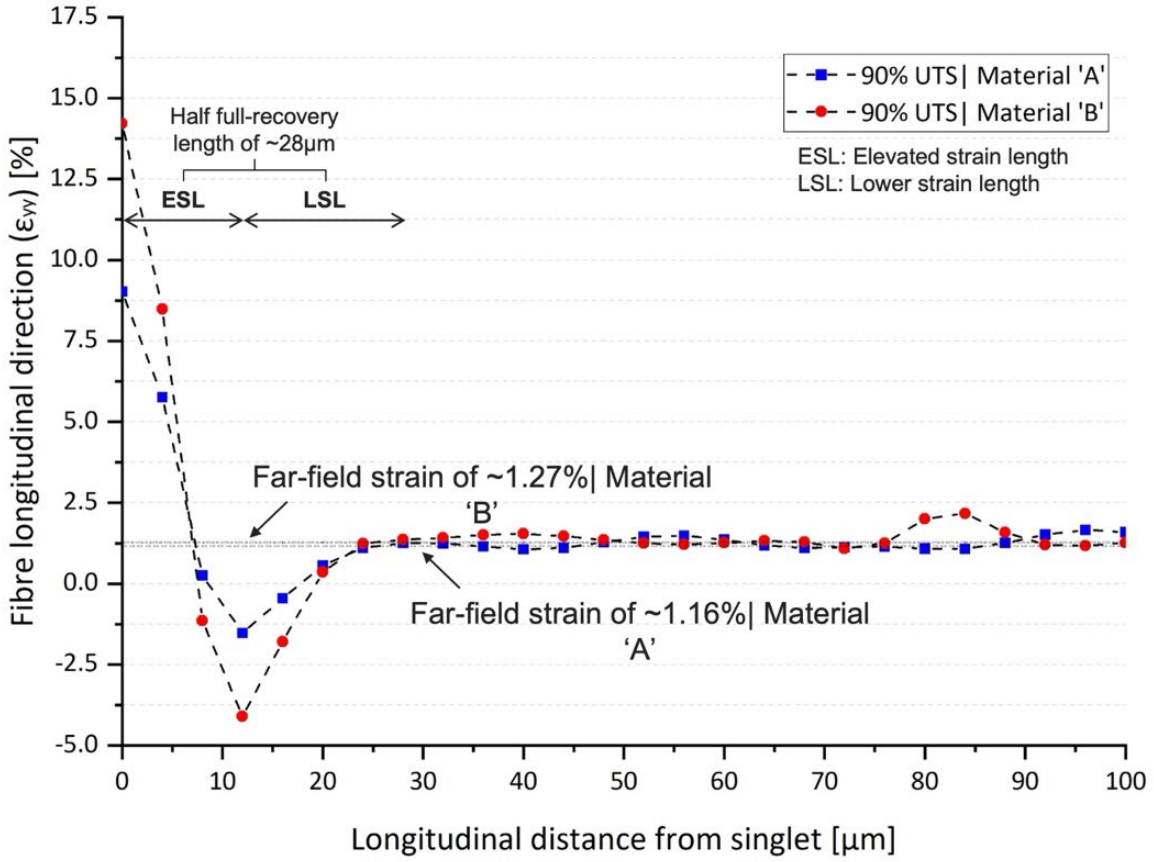

Fig. 8. Half of the longitudinal strain gradients of both material 'A' and 'B' obtained by folding strain measurements around individual breaks (averaging value from equidistance top and bottom regions) and averaging strains across 8 singlet sites at the 90% UTS level

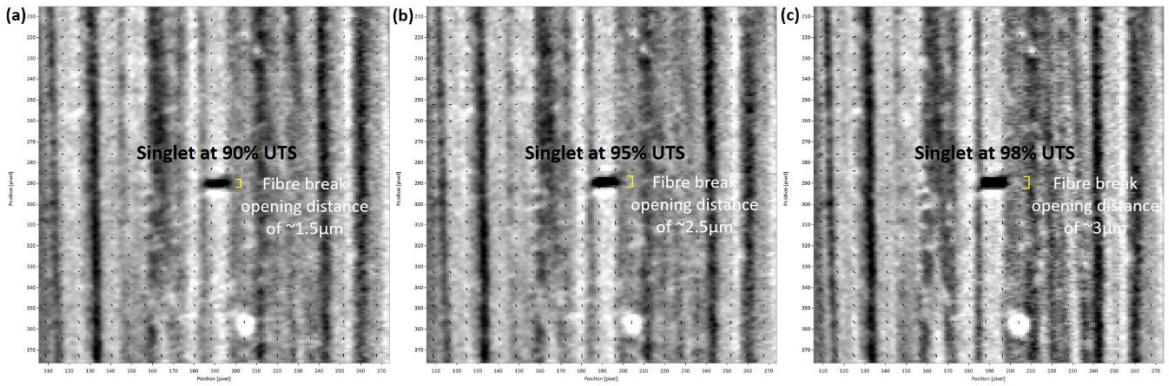

Fig. 9. Evolution of singlet of material 'B' with increasing opening distance for the (a) 90% UTS level, (b) 95% UTS level, and (c) 98% UTS level.

5 CONCLUSIONS AND FUTURE WORK

This DVC work, combined with *in situ* SRCT, demonstrates the assessment of strain fields longitudinally from fibre breaks in SiO_2 doped CFRPs with two different surface treatment types subjected to quasi-static tensile loading. It can be observed that the use of industrial-grade SiO_2 particles not only provides a comparable level of DVC performance to a previous study using $BaTiO_3$ particles, but also achieves improved particle distribution with reduced agglomeration. The longitudinal strains from singlets at the 90% UTS level resulted in similar strain-recovery lengths of ~56 μm in both the materials investigated. Overall, the resulting shorter full-recovery length in comparison to a $BaTiO_3$ doped CFRPs suggested faster strain recovery at occurring fibre breaks. However, a limitation exists in that the measured strains should be understood as an output encompassing the spatial filtering of the DVC algorithm, deformation gradients in both the fibre and matrix, as well as various damage mechanisms within a sub-volume. Notwithstanding careful interpretation of specific strain values, it is noted that determination of the distance at which strains recover to background levels is based on measurements *away* from actual breaks sites, and is therefore less susceptible to correlation and strain gradient issues. The ongoing research is being extended to assess longitudinal strain measurements for a range of fibre breaks clusters.

ACKNOWLEDGEMENTS

The authors would like to acknowledge the contributions from the Mitsubishi Chemical Corporation (Advanced Molding and Composites Laboratory, Aichi R&D centre, Japan) and the dedicated MCC scientists – Mr. Fukuhara Yasuhiro, Mr. Takano Tsuneo, Mr. Sugiura Naoki – for their sponsorship, material supplies, and technical support. The authors also recognise the Super Photon ring-8 GeV (Spring-8) BL20XU beamline for provision of synchrotron radiation facilities and would like to appreciate the beamline scientists – Dr. Akihisa Takeuchi and Dr. Masayuki Uesugi – for their beamline set-up and assistance in using BL20XU. The authors also gratefully acknowledge the μ-VIS X-Ray Imaging Centre at the University of Southampton for providing dedicated high-speed computational facilities. A huge acknowledgment is given to Dr. Erich Schöberl for advice on experiment preparation and extensive technical support in using digital volume correlation techniques. Credit is further extended to Mr. Simon Beever of the University of Southampton Engineering Design and Manufacturing Centre (EDMC) for the precise water-jet cutting of various components.

REFERENCES

[1] E. Schöberl *et al.*, "Fibre-direction strain measurement in a composite ply under quasi-static tensile loading using Digital Volume Correlation and in situ Synchrotron Radiation Computed Tomography," *Composites Part A: Applied Science and Manufacturing,* vol. 137, p. 105935, 2020.

[2] E. Schöberl, M. Mavrogordato, I. Sinclair, and S. Spearing, "Fibre direction strain measurement in a composite ply under pure bending using Digital Volume Correlation and Micro-focus Computed Tomography," *Journal of Composite Materials,* vol. 54, no. 14, pp. 1889-1912, 2020.

[3] P. Wright, A. Moffat, I. Sinclair, and S. Spearing, "High resolution tomographic imaging and modelling of notch tip damage in a laminated composite," *Composites science and technology,* vol. 70, no. 10, pp. 1444-1452, 2010.

[4] P. Wright, X. Fu, I. Sinclair, and S. Spearing, "Ultra high resolution computed tomography of damage in notched carbon fiber—epoxy composites," *Journal of composite materials,* vol. 42, no. 19, pp. 1993-2002, 2008.

[5] E. Schöberl *et al.*, "A novel particle-filled carbon-fibre reinforced polymer model composite tailored for the application of digital volume correlation and computed tomography," *Journal of Composite Materials,* vol. 55, no. 14, pp. 1907-1934, 2021.

[6] S. Rosini, M. N. Mavrogordato, T. Takano, N. Sugiura, S. M. Spearing, and I. Sinclair, "Fibre failure assessment in carbon fibre reinforced polymers under tensile loading using in situ synchrotron X-ray computed tomography," (in English), *Journal of Composite Materials,* vol.

56, no. 6, pp. 825-836, Mar 2022, doi: Artn 00219983211061900 10.1177/00219983211061900.

[7] S. Rosini *et al.*, "In situ statistical measurement of local morphology in carbon-epoxy composites using synchrotron X-ray computed tomography," (in English), *Compos Part a-Appl S,* vol. 125, Oct 2019, doi: ARTN 105543 10.1016/j.compositesa.2019.105543.

[8] 3M™. "Data Sheets- 3M Scotch-Weld™ Structural Epoxy Adhesive EC-9323 B/A." https://multimedia.3m.com/mws/media/2157921O/3m-ec-9323-ba-structural-epoxy-paste-adhesive-tds.pdf (accessed.

[9] A. Scott, "Analysis of a hybrid composite pressure vessel using multi-scale computed tomography techniques," Doctoral Thesis, University of Southampton, 2011.

[10] M. P. Fernandez, A. H. Barber, G. W. Blunn, and G. Tozzi, "Optimization of digital volume correlation computation in SR-microCT images of trabecular bone and bone-biomaterial systems," (in English), *J Microsc-Oxford,* vol. 272, no. 3, pp. 213-228, Dec 2018, doi: 10.1111/jmi.12745.

[11] B. K. Bay, "Methods and applications of digital volume correlation," (in English), *J Strain Anal Eng,* vol. 43, no. 8, pp. 745-760, Nov 2008, doi: 10.1243/03093247jsa436.

[12] F. Xu, "Quantitative characterization of deformation and damage process by digital volume correlation: A review," *Theoretical and Applied Mechanics Letters,* vol. 8, no. 2, pp. 83-96, 2018.

[13] G. Borstnar, F. Gillard, M. N. Mavrogordato, I. Sinclair, and S. M. Spearing, "Three-dimensional deformation mapping of Mode I interlaminar crack extension in particle-toughened interlayers," (in English), *Acta Mater,* vol. 103, pp. 63-70, Jan 15 2016, doi: 10.1016/j.actamat.2015.09.059.

[14] S. Yaofeng and J. H. Pang, "Study of optimal subset size in digital image correlation of speckle pattern images," *Optics and lasers in engineering,* vol. 45, no. 9, pp. 967-974, 2007.

[15] J. Schindelin *et al.*, "Fiji: an open-source platform for biological-image analysis," *Nature methods,* vol. 9, no. 7, pp. 676-682, 2012.